electronics

Article

A Multi-Model Architecture Based on Deep Learning for Longitudinal Available Overload Prediction of Commercial Subsonic Aircraft with Actuator Faults

Shengqiang Shan [1], Yuehua Cheng [1,*], Bin Jiang [1], Cheng Xu [2], Kun Guo [2] and Xingyu Lin [1]

[1] College of Automation, Nanjing University of Aeronautics and Astronautics, Nanjing 211106, China; ssq123@nuaa.edu.cn (S.S.); binjiang@nuaa.edu.cn (B.J.); linxingyu@nuaa.edu.cn (X.L.)
[2] Beijing Institute of Mechanical and Electrical Engineering, Beijing 100074, China; xch2000_1980@163.com (C.X.); 2007guokun@163.com (K.G.)
* Correspondence: chengyuehua@nuaa.edu.cn

Abstract: Assessing the real-time longitudinal available overload onboard under fault conditions offers vital insights for the fault-tolerant reconfiguration and trajectory planning of commercial subsonic aircraft. After actuator failures in a commercial subsonic aircraft, its aerodynamic model undergoes changes. Traditional methods based on analytical models rely on precise aerodynamic models. However, due to the complexities of the flight environment and uncertainties in disturbances, establishing an accurate aerodynamic model after actuator failures is often challenging. Consequently, traditional methods can yield significant errors when evaluating the available overload under actuator faults. To address this, we introduce a multi-model architecture based on deep learning for the longitudinal available overload prediction of a commercial subsonic aircraft with actuator faults. For flight state data under different working conditions and different faults, Spearman correlation coefficient analysis and the gradient boosting decision tree (GBDT) algorithm are used to remove redundant feature parameters, thereby enhancing the training and prediction speed of the model while reducing the risk of overfitting. To meet prediction accuracy and speed demands, we employ the multi-layer perceptron (MLP) deep learning network to fully explore the environmental features, including uncertainties and disturbances, within the flight state, and the mapping relationships between the flight state and the available overload variations. We incorporate the light gradient boosting machine (LightGBM) and the categorical boosting (CatBoost) algorithms to enhance the model's prediction speed and fuse it with a longitudinal available overload analytical model to elevate the model's prediction accuracy, thereby achieving the real-time estimation of the commercial subsonic aircraft's longitudinal available overload with actuator faults. The results demonstrate that the proposed method achieves a higher accuracy than traditional methods, with a relative error of less than 5%.

Keywords: flight capability assessment; actuator fault; longitudinal available overload; MLP deep learning network

Citation: Shan, S.; Cheng, Y.; Jiang, B.; Xu, C.; Guo, K.; Lin, X. A Multi-Model Architecture Based on Deep Learning for Longitudinal Available Overload Prediction of Commercial Subsonic Aircraft with Actuator Faults. *Electronics* **2024**, *13*, 3723. https://doi.org/10.3390/electronics13183723

Academic Editor: Felipe Jiménez

Received: 2 August 2024
Revised: 31 August 2024
Accepted: 4 September 2024
Published: 19 September 2024

1. Introduction

For commercial subsonic aircraft engaged in long-term missions, factors such as wear and tear, poor maintenance, and environmental conditions may lead to actuator faults [1,2], sensor faults [3,4], and electronic device failures [5]. Actuator faults [6,7], such as being stuck, looseness, and damage, restrict the deflection of the commercial subsonic aircraft's control surfaces and alter its aerodynamic configuration, subsequently reducing the available overload post-fault and impairing the commercial subsonic aircraft's maneuverability. Longitudinal available overload, a key metric for evaluating maneuverability, requires timely and accurate predictions post-fault to support fault-tolerant control and mission planning [8,9].

The assessment of flight performance includes the evaluation of a wide range of capabilities, including aircraft control performance, range capability, and maneuverability. The majority of existing research in this field has focused on the analysis of normal flight conditions. Methods employed include index evaluation, analytical methods, and machine learning-based approaches. Index evaluation is primarily used for multi-index tasks such as control performance assessment [10,11], involving the establishment of evaluation index systems [12], weighting techniques [13], and the selection of evaluation methods [14,15]. Analytical methods are typically applied to single-index evaluations, such as range capability [16,17] and maneuverability [18,19]. In light of the accelerated development of artificial intelligence, an ever-growing number of scholars are utilizing machine learning methods in flight performance assessments. Control performance [20], range capability [21], and maneuverability [22,23] can all be evaluated using machine learning, though this approach often requires extensive and highly reliable datasets [24].

The existing literature on the evaluation of aircraft maneuverability is relatively sparse, focusing primarily on analytical methods and machine learning-based approaches. Studies [18,19] employ analytical methods to solve for aircraft maneuverability by fitting parameters under certain conditions into algebraic functions within the equations of motion for the aircraft as a particle. Analytical methods depend on precise aircraft models, which can lead to significant errors if the model changes or includes disturbances and uncertainties. Studies [22,23] are based on a substantial corpus of flight experimental data and employ statistical distribution or neural network methods to predict the aircraft's maneuvering capability.

The existing methods for evaluating maneuverability demonstrate good accuracy when the aircraft is in a fault-free state. Traditional overload assessment methods mostly rely on accurate aerodynamic analysis models; however, when an aircraft malfunctions, its aerodynamic model also changes accordingly. Due to the complexity of the flight environment and the uncertainty of disturbances, it is often difficult to establish an accurate aerodynamic analysis model after actuator failure. Therefore, traditional overload assessment methods can generate significant errors when evaluating the available overload under actuator faults. To address this issue, this paper proposes a multi-model architecture based on deep learning for the longitudinal available overload prediction of a commercial subsonic aircraft with actuator faults. This model addresses the need for rapid and accurate in-orbit performance prediction, analyzing flight state changes and data characteristics under various actuator fault conditions. It selects targeted deep networks to mine the impact of actuator faults on flight state, aerodynamic model, and control surface effectiveness changes. Combining feature dimensionality reduction and rule fusion algorithms, a prediction model for longitudinal available overload under actuator fault conditions is established.

The remainder of this paper is organized as follows: First, a mathematical description of the problem is provided. Then, a deep learning algorithm integrated with multiple models for predicting longitudinal available overload under actuator fault conditions is proposed. Next, simulation validation is presented, along with a comparison and analysis of the experimental results. Eventually, conclusions are drawn from the findings.

2. Problem Description

2.1. Analytical Model

When establishing the model of the longitudinal available overload prediction of a commercial subsonic aircraft with actuator faults, it is desired to unify the formula derivation in a single frame, namely the body frame for example. In order to clarify the derivation process, Figure 1 shows the relationship between the body frame and other frames, as well as the representation of correlated parameters. The meanings of these parameters will be presented below, and the specific definitions are not further elaborated for the sake of simplicity.

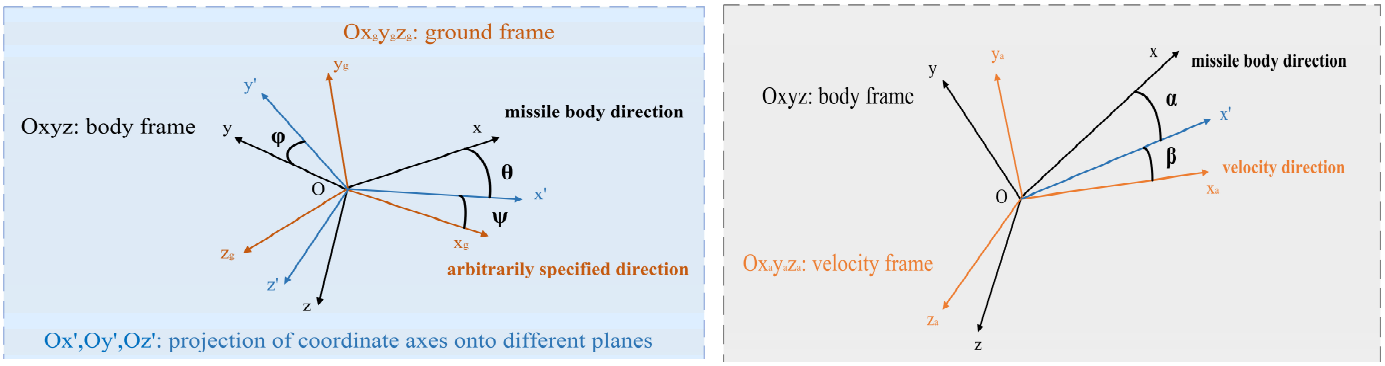

(**a**) (**b**)

Figure 1. Relationship between different frames and correlated parameters. (**a**) Body frame and ground frame. (**b**) Body frame and velocity frame.

Commercial subsonic aircraft available overload is a critical parameter for evaluating commercial subsonic aircraft maneuverability during flight. It is defined as the overload a commercial subsonic aircraft can generate when the actuator is deflected to its limit position and the commercial subsonic aircraft is in a balanced state [18]. When a fault occurs in the commercial subsonic aircraft's actuator, the deflection range of the control surface changes, and the aerodynamic configuration is altered, resulting in a reduction in the commercial subsonic aircraft's available overload.

Assuming no sideslip during commercial subsonic aircraft flight and engine thrust along the flight velocity direction, let the resultant external force on the commercial subsonic aircraft in the pitch plane at time k, excluding gravity, be $N_y(k)$, and the longitudinal overload be $n_y(k)$. We obtain the following:

$$n_y(k) = \frac{N_y(k)}{m(k)g(k)} = \frac{P(k)\sin\alpha(k) + Y(k)}{m(k)g(k)} \tag{1}$$

where $m(k)$, $g(k)$, $\alpha(k)$, $Y(k)$, and $P(k)$ represent the commercial subsonic aircraft's mass, gravitational acceleration, angle of attack, lift force, and engine thrust at time k, respectively.

The term Y in Equation (1) can be computed using the following equation:

$$\begin{cases} Q(k) = \frac{1}{2}\rho(k)V^2(k) \\ Y(k) = C_Y(k)Q(k)S \end{cases} \tag{2}$$

where $Q(k)$, $\rho(k)$, $V(k)$, and $C_Y(k)$ denote the dynamic pressure, air density, flight speed, and lift coefficient at time k, and S is the reference area.

The term C_Y in Equation (2) can be derived from ground experiments, typically expressed as follows [25]:

$$C_Y(k) = f_{C_Y}(V(k), h(k), \alpha(k), \delta_y(k)) \tag{3}$$

where $h(k)$ and $\delta_y(k)$ are the commercial subsonic aircraft's flight altitude and elevator deflection angle at time k, respectively.

Based on the "instantaneous equilibrium" assumption for commercial subsonic aircraft [18], we obtain the following:

$$C_{M_z}(k) = f_{M_z}(V(k), h(k), \alpha(k), \delta_y(k)) = 0 \tag{4}$$

where $C_{M_z}(k)$ is the pitching moment coefficient at time k, which can also be derived from ground experiments. Further derivation yields the following:

$$\alpha(k) = f_\alpha(V(k), h(k), \delta_y(k)) \tag{5}$$

Combining Equations (1)–(5), we obtain the following:

$$n_y^p(k) = \frac{P(k)\sin(f_\alpha(V(k), h(k), \delta_y^{\text{limit}})) + \frac{1}{2}\rho(k)V^2(k)C_Y(k)S}{m(k)g(k)} \tag{6}$$

where δ_y^{limit} is the maximum deflection angle of the commercial subsonic aircraft's elevator at time k.

2.2. Problem Analysis

Assume an actuator fault occurs at time $k(k > 0)$, with the measurable flight state information being $X = \{X(1), X(2), \ldots, X(k)\}$, where $X(t), t \in [1, k]$ is the measurable flight state vector at time t. The fault information is $\xi = \{\xi_\lambda, \xi_\delta, \xi_\kappa\}$, where ξ_λ denotes the fault type, ξ_δ denotes the faulty rudder, and ξ_κ denotes the fault severity. At time k, the commercial subsonic aircraft's longitudinal available overload in the absence of a fault is $n_y^p(k)$, and the change in the longitudinal available overload due to the actuator fault is $f_{\Delta n_y^p}(\{X(1), X(2), \ldots, X(k)\}, \{\xi_\lambda, \xi_\delta, \xi_\kappa\})$.

At time k, let $\Delta_\xi^{C_Y}$ and $C_{M_z}^\Delta(k)$ be the changes in the lift coefficient and pitching moment coefficient due to actuator faults, respectively. We obtain the following:

$$C_Y^\Delta(k) = f_{C_Y}(V(k), y(k), \alpha(k), \delta_y(k)) + \Delta_\xi^{C_Y}(X, \xi) \tag{7}$$

$$C_{M_z}^\Delta(k) = f_{M_z}(V(k), y(k), \alpha(k), \delta_z(k)) + \Delta_\xi^{M_z}(X, \xi) = 0 \tag{8}$$

where $C_Y^\Delta(k)$ and $C_{M_z}^\Delta(k)$ are the lift coefficient and pitching moment coefficient at time k, influenced by environmental disturbances, uncertainties, and actuator faults, respectively.

Assuming the longitudinal available overload of the commercial subsonic aircraft at time k, influenced by environmental disturbances, uncertainties, and actuator faults, is $n_y^\xi(k)$, combining Equations (1)–(8) yields the following:

$$\begin{aligned} n_y^\xi(k) &= n_y^p(k) + \Delta n_y^p(k) \\ &= n_y^p(k) + f_{\Delta n_y^p}(\{X(1), X(2), \ldots, X(k)\}, \{\xi_\lambda, \xi_\delta, \xi_\kappa\}) \end{aligned} \tag{9}$$

From the above derivation, it can be seen that the traditional analytical method for solving available overload under fault conditions faces two challenges: (1) precise models for environmental disturbances and uncertainties are difficult to establish; (2) accurate aerodynamic models of commercial subsonic aircraft after multiple actuator faults are hard to obtain. Considering that the impact of environmental disturbances, uncertainties, and actuator faults on longitudinal available overload is embedded in the measurable flight state data and fault information, this paper adopts a research approach based on deep learning networks to fully explore the changes in longitudinal available overload contained within the flight state data and fault information.

3. Proposed Method

Based on the derivations and analysis in Section 2, the multi-model for predicting the longitudinal available overload of a commercial subsonic aircraft with actuator faults consists of two main components (as shown in Figure 2a). One component utilizes the analytical model to compute $n_y^p(k)$, while the other relies on deep learning networks for the real-time prediction of $\Delta n_y^p(k)$. The construction flowchart of the multi-model for predicting the longitudinal available overload of a commercial subsonic aircraft under faults is depicted in Figure 2, with the primary steps as follows:

(1) Conduct wind tunnel simulation experiments on a commercial subsonic aircraft in a normal state to obtain a precise aerodynamic model of the commercial subsonic aircraft under non-fault conditions. Based on this, derive the analytical model for

computing the longitudinal available overload by integrating the commercial subsonic aircraft's dynamics and kinematics models.

(2) Construct datasets of commercial subsonic aircraft flight states under different types of actuator faults. First, preprocess the datasets as shown in Figure 2b: (1) perform data cleaning on the flight state data to remove anomalous trajectory data; (2) normalize and standardize the flight state data. Then, conduct feature dimensionality reduction using the Spearman method andGBDT algorithm, as illustrated in Figure 2c: (1) utilize Spearman correlation analysis to identify and selectively remove flight state parameters with strong correlations within the dataset; (2) apply the GBDT algorithm to filter out redundant flight state parameters that do not contribute to the longitudinal available overload variation and eliminate them.

(3) Based on the processed different actuator fault datasets from step (2), construct predictive models for the longitudinal available overload variation under actuator faults using MLP, LightGBM, and CatBoost. Then, set the model fusion rules, according to accuracy and speed requirements, to obtain the integrated model for the real-time prediction of $\Delta n_y^p(k)$ with actuator faults.

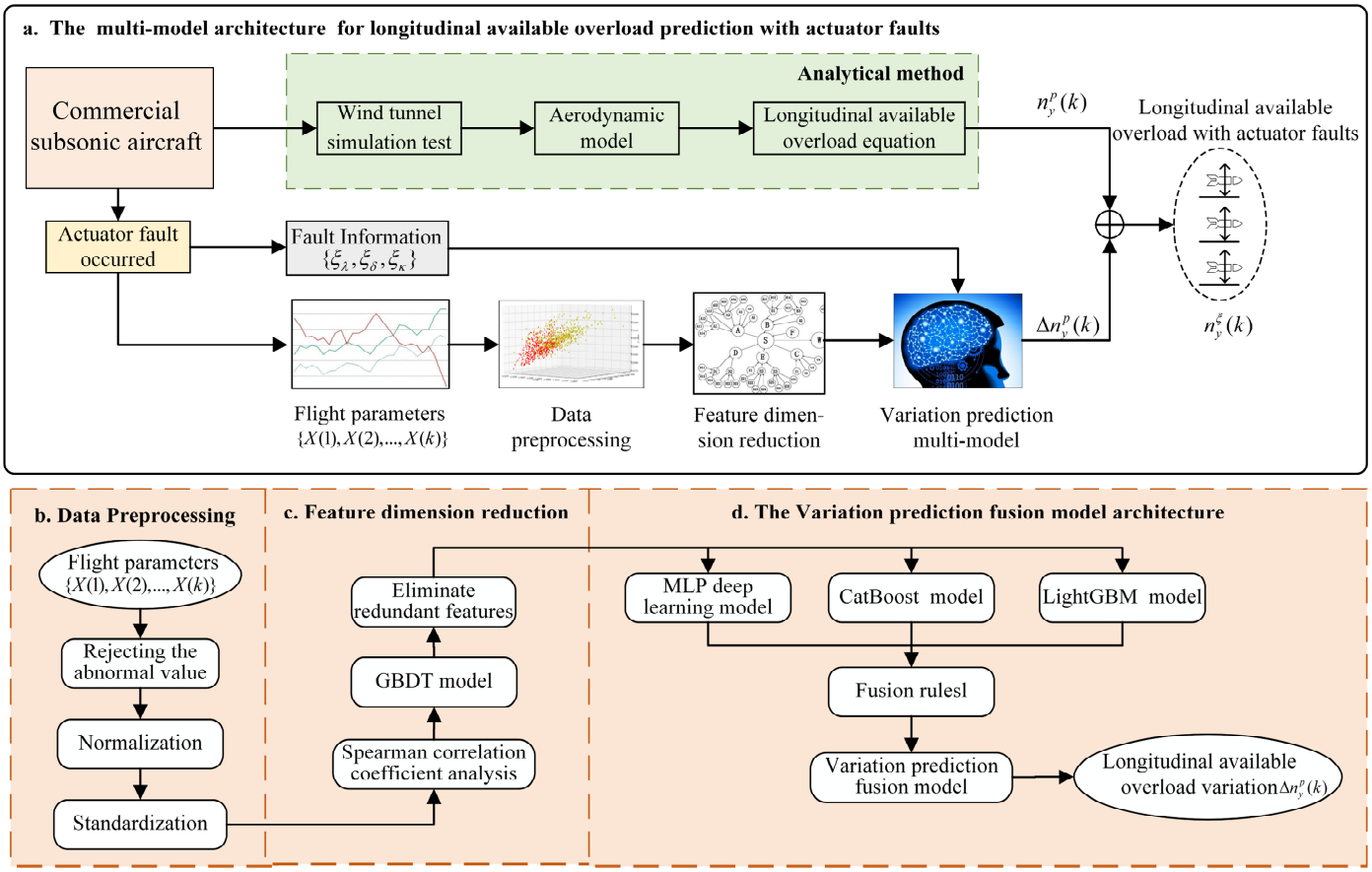

Figure 2. Flowchart for predicting longitudinal available overload of commercial subsonic aircraft with actuator faults.

3.1. Analysis Model of Longitudinal Available Overload for Commercial Subsonic Aircraft

Initially, we model the aerodynamic shape of the commercial subsonic aircraft, followed by wind tunnel simulation experiments, based on this model, to derive the aerodynamic parameter fitting model. Taking the BGM-109D commercial subsonic aircraft as an example, its aerodynamic parameter fitting model is shown in Equations (10) and (11) [25].

It is important to note that this linear fitting model maintains high accuracy only under the conditions of 240 m/s $\leq V \leq$ 300 m/s and 600 m $\leq H \leq$ 1000 m.

$$C_Y = C_{Y0} + C_{Y\alpha} \cdot \alpha + C_{\delta_z} \cdot (\delta_1 - \delta_2 - \delta_3 + \delta_4) \tag{10}$$

where C_{Y0} is the lift coefficient at a zero angle of attack and elevator deflection, $C_{Y\alpha}$ is the stability derivative of the lift coefficient with respect to the angle of attack, and $C_{\delta_z} \approx 0$ are the stability derivatives of the lift coefficient with respect to the deflection angles of the four control surfaces.

$$C_{M_z} = C_{M_z\ 0} + C_{M_z\ \alpha} \cdot \alpha + C_{M_z\ \delta 0} \cdot (\delta_1 - \delta_2 - \delta_3 + \delta_4) \tag{11}$$

where $C_{M_z\ 0}$ is the pitching moment coefficient at a zero angle of attack, sideslip angle, and deflection, $C_{M_z\ \alpha}$ is the stability derivative of the pitching moment coefficient with respect to the angle of attack, and $C_{M_z\ \delta 0}$ is the stability derivative of the pitching moment coefficient with respect to the elevator deflection angle.

For ease of calculation, we assume α is small, so $\sin\alpha \approx \alpha$ [18]. According to Equation (6), we obtain the following:

$$n_y^p = \frac{1}{m \cdot g} Q \cdot S \cdot C_{Y_0} - (P + Q \cdot S \cdot C_{Y_\alpha}) \cdot \frac{C_{m0} + C_{m\delta 0} \cdot (\delta_1 - \delta_2 - \delta_3 + \delta_4)_{\mathrm{lim}it}}{m \cdot g \cdot C_{m\alpha}} \tag{12}$$

This equation represents the analytical model for the commercial subsonic aircraft's longitudinal available overload, applicable under fault-free conditions.

3.2. Feature Dimension Reduction Based on Spearman–GBDT Algorithm

The commercial subsonic aircraft actuator fault dataset presents the following issues: (1) there is a strong correlation between different flight parameters in the dataset, leading to redundant contributions from various feature parameters in predicting changes in longitudinal available overload; (2) the dataset has high dimensionality, containing redundant parameters that do not contribute to the longitudinal available overload variation. To address issue (1), the Spearman correlation coefficient [26] is used to identify strongly correlated flight state parameters in the dataset. This method can quantify the trend in changes between flight state parameters and is more suitable for measuring nonlinear relationships than the more commonly used Pearson correlation coefficient. It also performs better on datasets with outliers [27]. To address issue (2), the GBDT algorithm is employed to filter out redundant flight state parameters that do not contribute to the longitudinal available overload variation. This algorithm has high accuracy on complex datasets with high dimensionality and nonlinear relationships [28].

(1) Feature Correlation Analysis Based on Spearman Correlation Coefficient [29]

Suppose that the ranks of two different flight state parameters $x_i (i = 1, 2, \ldots, n)$ and $y_i (i = 1, 2, \ldots, n)$ in the dataset are rkx_i and rky_i, respectively. The Spearman correlation coefficient c_s between them is as follows:

$$c_{\mathrm{s}} = \frac{\mathrm{cov}(rkx_i, rky_i)}{\sigma_{rkx_i} \sigma_{rky_i}} \tag{13}$$

where $\mathrm{cov}(rkx_i, rky_i)$ is the covariance between rkx_i and rky_i, and σ_{rkx_i} and σ_{rky_i} are the standard deviations of rkx_i and rky_i, respectively. The closer the absolute value of $c_{\mathrm{s}} (-1 < c_{\mathrm{s}} < 1)$ is to one, the stronger the correlation between the two flight state parameters is.

(2) Feature Importance Analysis Based on GBDT Algorithm

In the GBDT feature importance analysis, the Gini index (GI) is used to measure the importance of each input flight feature parameter. The GI value is obtained by averaging the values of each feature in every tree of the algorithm. Suppose there are n flight feature

parameters in the dataset, denoted as $X = \{x_1, x_2, \ldots, x_n\}$. The Gini index calculation formula is as follows [30]:

$$GI_v^{(i)} = \sum_{c=1}^{|c|} \sum_{c \neq c} p_{vc}^{(i)} p_{vc}^{(i)} = 1 - \sum_{c=1}^{|c|} \left(p_{vc}^{(i)}\right)^2 \tag{14}$$

where $GI_v^{(i)}$ refers to the purity of the i-th tree node v, c denotes the class of the data sample, and p_{vc} denotes the proportion of class c records for node v. The importance score (VIM) of flight feature parameter x_j is calculated as follows:

$$VIM_{jv}^{(Gini)(i)} = GI_v^{(i)} - \left[GI_l^{(i)} + GI_r^{(i)}\right] \tag{15}$$

where l and r are the left and right child nodes of node v, and $GI_l^{(i)}$ and $GI_r^{(i)}$ represent the Gini indices of nodes l and r, respectively. The variable importance score for the i-th tree is given by Equation (16), where Q is the total number of nodes in the i-th tree. Suppose the total number of trees is m, then the total importance score of the flight feature parameter in m trees is given by Equation (17) [31], as follows:

$$VIM_j^{(Gini)(i)} = \sum_{v \in Q} VIM_{jv}^{(Gini)(i)} \tag{16}$$

$$VIM_j^{(Gini)} = \sum_{i=1}^{m} VIM_j^{(Gini)(i)} \tag{17}$$

Finally, the obtained feature importance scores are normalized, as shown in Equation (18):

$$VIM_{sj}^{(Gini)} = \frac{VIM_j^{(Gini)}}{\sum_{j=1}^{n} VIM_j^{(Gini)}} \tag{18}$$

where $VIM_j^{(Gini)}$ refers to the Gini index of the j-th flight feature parameter, $\sum_{j=1}^{n} VIM_j^{(Gini)}$ refers to the summation of the GI of all flight feature parameters, and $VIM_{sj}^{(Gini)}$ refers to the GBDT feature importance of the j-th flight feature parameter after normalization; the smaller the value of $VIM_{sj}^{(Gini)}$, the less the contribution of the flight feature parameter to the prediction result.

3.3. Fusion Model for Predicting $\Delta n_y^p(k)$

Figure 2d illustrates the fusion model architecture of the longitudinal available overload variation prediction with actuator faults. The input to this model is the processed time-series data of flight states under actuator fault conditions, and the output is the longitudinal available overload variation after an actuator fault occurs. This model is constructed based on the MLP deep neural network. MLP is a type of deep neural network that forms a complex network structure through extensive interconnections of numerous simple neuron processing units. When the flight state data are sufficiently balanced, the deep learning network constructed by MLP can fully learn the impact of actuator faults on the longitudinal available overload contained in the flight state data, enabling the accurate prediction of this impact.

Given the airborne algorithm's requirement for rapid performance, the LightGBM and CatBoost networks, both known for their outstanding predictive speed [32,33], are introduced. Since the datasets obtained under different actuator faults have varying data characteristics, to meet the accuracy and speed requirements of the airborne model, the

three networks are trained separately on each fault dataset to obtain multiple models for predicting the longitudinal available overload variation under different actuator faults.

As commercial subsonic aircraft are complex nonlinear systems with high stability and safety requirements during flight [34], the airborne flight maneuver performance evaluation system needs to provide quick and accurate predictions of longitudinal available overload to minimize significant prediction deviations. Therefore, the following three criteria are introduced to integrate the multiple models for predicting longitudinal available overload variation under actuator faults:

(1) Speed Criterion: The model's single-point prediction time must be less than t_s;
(2) Minimal Maximum Deviation Criterion: If there exists a model with a maximum relative error less than γ, select according to Criterion 3; if not, select the model with the smallest maximum relative error;
(3) Accuracy Criterion: If multiple models simultaneously satisfy Criteria 1 and 2, select the model with the smallest average relative error.

The parameters t_s and γ in the above three criteria can be flexibly chosen according to different mission requirements.

4. Experimental Validation

4.1. Dataset

In order to verify the applicability of the proposed algorithm, the BGM-109D commercial subsonic aircraft was taken as the research object, and its model was established on the Simulink simulation platform. As shown in Figure 3, the commercial subsonic aircraft model consists of six modules: dynamics and kinematics, engine, rudder, control system, navigation system, and guidance system. To align with real flight scenarios, the wind module in the simulation employs the Dryden Wind Turbulence model and wind shear model; the environmental model utilizes the 1976 International Standard Atmosphere model; and the gravity model is based on the gravity calculation model from the World Geodetic System. To ensure that the algorithm effectively accommodates various flight states under different actuator failures, target flight points were set within the ranges specified in Table 1, and actuator failure parameters were established within the ranges outlined in Table 2, thereby generating diverse fault datasets. The measurable flight parameters obtained are listed in Table 3.

Table 1. Flight parameter settings for fault dataset.

	Target Height	Target Speed	Initial Mass
Traverse Range	600 m~1000 m	200 m/s~280 m/s	1152 kg~1452 kg
Traverse Interval	20 m	20 m/s	25 kg

Table 2. Fault parameter settings of different fault datasets.

Fault Dataset	Fault Control Surface	Fault Severity	Number of Ballistic Data
No Fault	None	None	1365
Damage	Rudder 1, 2, 3, or 4	20%, 40%, 60%	16,380
Stuck	Rudder 1, 2, 3, or 4	5°, 10°	10,920
Loosing	Rudder 1, 2, 3, or 4	None	5460

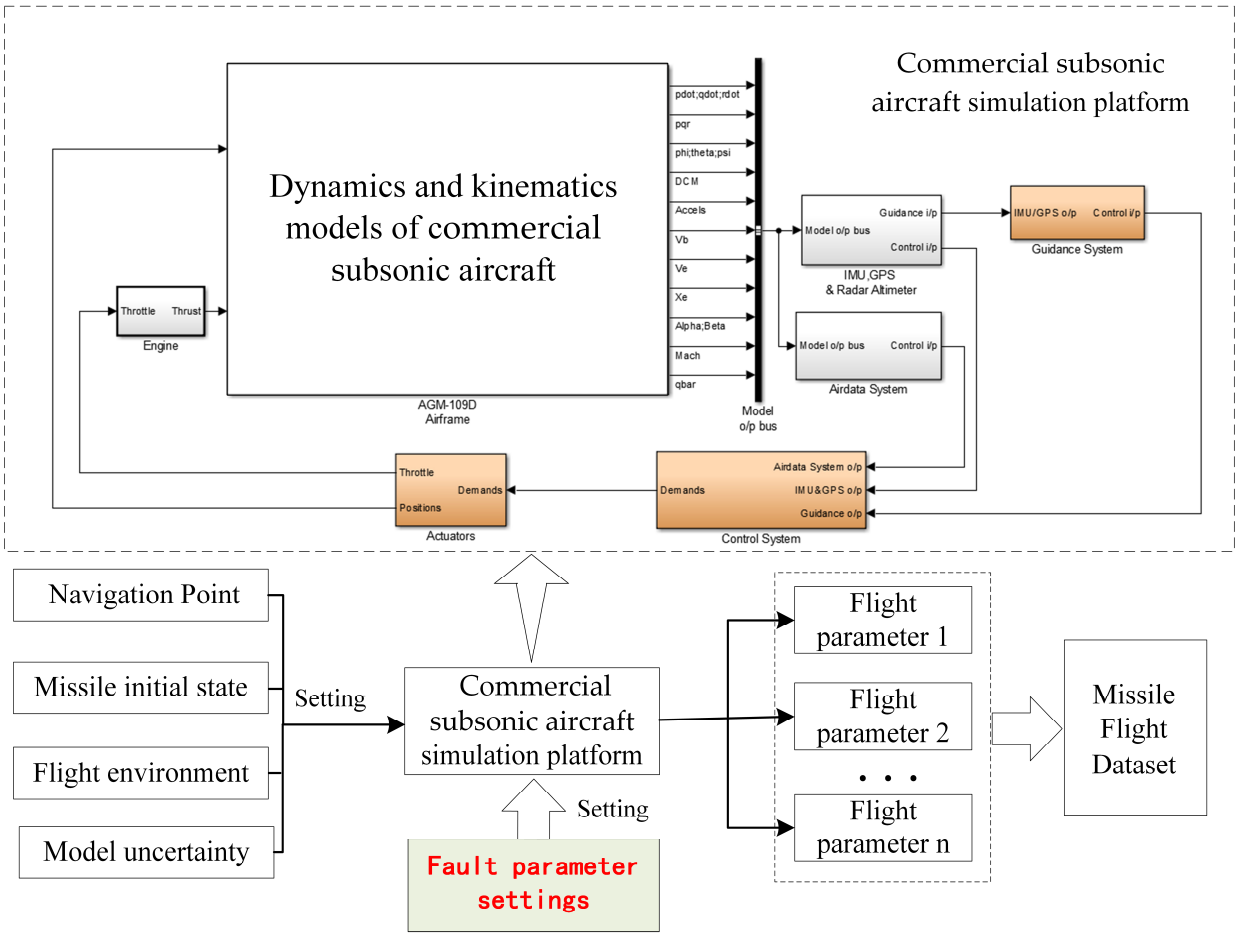

Figure 3. The BGM-109D commercial subsonic aircraft simulation system.

Table 3. Flight state parameters.

Variable Name	Meaning	Variable Name	Meaning	Variable Name	Meaning
x	Displacement along x-axis in Earth frame	y	Displacement along y-axis in Earth frame	z	Displacement along z-axis in Earth frame
v_x	Velocity along x-axis in body frame	v_y	Velocity along y-axis in body frame	v_z	Velocity along z-axis in body frame
a_x	Acceleration along x-axis in body frame	a_y	Acceleration along y-axis in body frame	a_z	Acceleration along z-axis in body frame
ϕ	Roll angle	ψ	Pitch angle	θ	Yaw angle
p	Roll rate	q	Yaw rate	r	Pitch rate
$\dot{p}$	Roll angular acceleration	$\dot{q}$	Yaw angular acceleration	$\dot{r}$	Pitch angular acceleration
α	Angle of attack	β	Sideslip angle	δ_1	Deflection angle of Rudder 1
δ_2	Deflection angle of Rudder 2	δ_3	Deflection angle of Rudder 3	δ_4	Deflection angle of Rudder 4
Ma	Mach number	m	Mass	ρ	Air density

Subsequently, we discarded trajectory data that did not control to the cruise target state at the time of fault occurrence. After screening, there were 921 abnormal trajectory data entries in the fault datasets. We then performed feature dimensionality reduction on the

fault datasets using the Spearman–GBDT algorithm. The process of feature dimensionality reduction was as follows:

(1) We conducted correlation analysis to calculate the Spearman correlation coefficients between feature variables. Figure 4 shows the heatmap of Spearman correlation coefficients among feature variables. We omitted one of the strongly correlated feature variables in the figure, which include x, z, a_y, a_z, and ψ.

(2) The importance of the remaining feature variables was calculated using GBDT, as shown in Figure 5. Features with a contribution to the prediction target less than or equal to 10^{-3}, namely variables θ, v_y, and ρ, were eliminated to reduce dimensional redundancy and enhance model training and prediction speed.

Figure 4. Heatmap of Spearman correlation coefficients among feature variables.

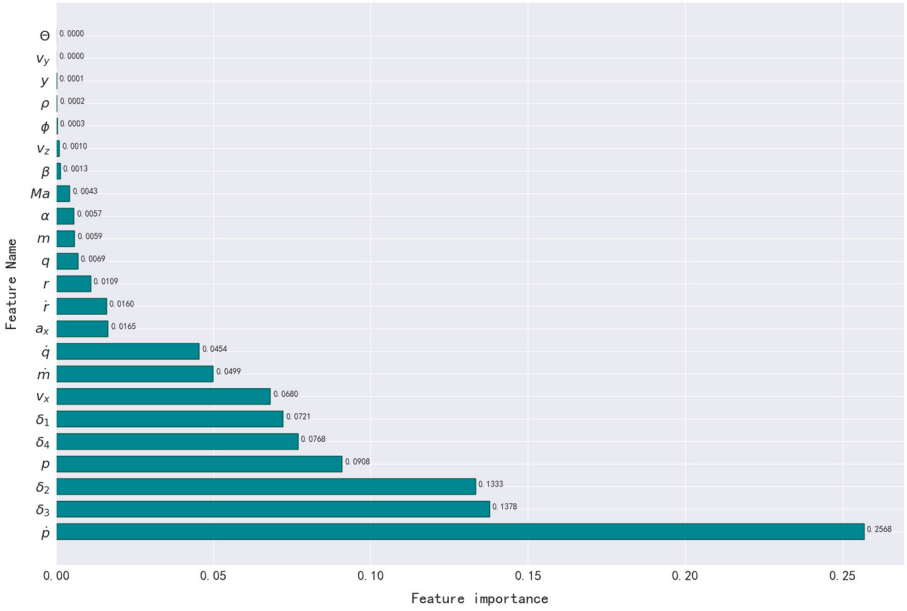

Figure 5. Feature importance results.

4.2. Prediction Model for $\Delta n_y^p(k)$ Results and Analysis

To reduce overfitting in the prediction model and enhance its generalization capabilities, we employed an exhaustive parameter search technique called grid search cross-validation (GSCV) [35]. The prediction model utilized fivefold cross-validation, with an 80%:20% ratio for the training and testing sets. The hyperparameters for the grid search are detailed in Table 4.

Table 4. Range of hyper-parameters for grid search.

Model	Hyper-Parameter	Range for Grid Search
MLP	Number of hidden layers	2, 3, 4, 5
	Number of neurons	100, 200, 300, 400
	Batch size	64, 128, 256
	Learning rate	0.05, 0.005
LightGBM	Number of leaves	20, 40, 60
	Number of boost round	1000, 5000, 10,000
	Learning rate	0.05, 0.005
CatBoost	Iterations	1000, 5000, 10,000
	Learning rate	0.05, 0.005
	Maximum depth	3, 6, 9

We trained longitudinal available overload variation prediction models using MLP deep learning networks, LightGBM networks, and CatBoost networks on different fault datasets, resulting in nine distinct models. These models were evaluated for accuracy and speed as follows:

(1) Accuracy Evaluation

The accuracy of the models was assessed using the mean absolute percentage error (MAPE) and the mean absolute error (MAE) [36,37]. The results are summarized in Table 5. As shown, during tests on damage and stuck fault datasets, the prediction model based on the MLP deep learning network achieved MAPEs of 0.18% and 0.22%, and MAEs of 0.0079 and 0.0034, respectively, outperforming the other two networks in terms of prediction accuracy. In tests on the looseness fault dataset, the prediction model trained with CatBoost had the lowest MAPE of 0.066%, while the model trained with LightGBM had the lowest MAE of 0.00069. This is due to the significantly larger sample size of damage and stuck fault datasets compared to the looseness fault dataset, where the MLP deep learning network generally performs better with larger datasets.

Table 5. Accuracy evaluation of different models for predicting $\Delta n_y^p(k)$.

Model	Metric	Damage	Stuck	Looseness
MLP	MAPE	0.18%	0.22%	0.23%
	MAE	0.0079	0.0034	0.0025
LightGBM	MAPE	0.43%	0.66%	0.060%
	MAE	0.0168	0.0099	0.00069
CatBoost	MAPE	0.20%	0.69%	0.066%
	MAE	0.0086	0.010	0.00076

(2) Relative Error Comparison of Different Models

The relative errors of each predictive model across different fault datasets were statistically analyzed and are shown in Figure 6. The conclusions drawn were as follows:

1. For the damage fault test set, over 99% of predictions from all three networks had errors within 5%, with very few exceeding this threshold.
2. For the stuck and looseness fault test sets, all predictions from the three networks had errors within 5%.

(3) Speed Evaluation of Different Models on Various Fault Test Sets

To evaluate real-time prediction capabilities, the average time taken by each model to predict a single data point in various fault test sets was measured. As shown in Table 6, the CatBoost network had the fastest prediction speed, while the MLP and LightGBM networks were relatively slower. This is due to the symmetrical tree structure and histogram-based optimization in CatBoost, which reduce parameters and enhance prediction efficiency [34].

Table 6. Speed evaluation of different models on various fault test sets.

Model	Damage	Stuck	Looseness
MLP	678.75 ms	457.10 ms	450.38 ms
LightGBM	466.53 ms	492.55 ms	420.80 ms
CatBoost	370.32 ms	196.60 ms	173.37 ms

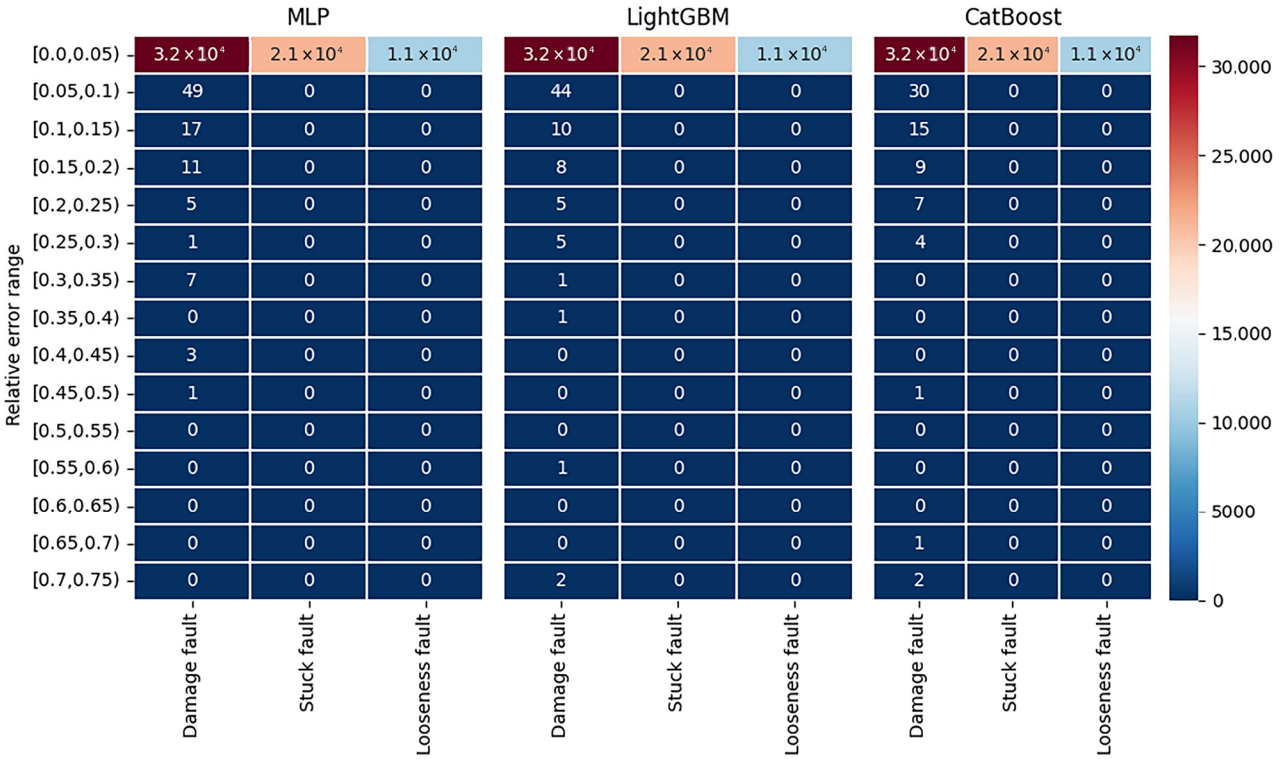

Figure 6. Relative error statistics of different models for predicting $\Delta n_y^p(k)$ on various fault test sets.

(4) Fusion of Longitudinal Available Overload Variation Prediction Models

Based on the three model fusion rules in Section 3.2, the longitudinal available overload variation prediction models were selected for different fault types, as shown in Table 7.

From Table 7, it is evident that LightGBM and CatBoost were equally chosen for defect fault models due to the diverse conditions in the defect fault dataset. The MLP network, while more accurate, was slower due to its complex structure and is thus unsuitable for real-time predictions. In the jamming fault dataset, the MLP model exceled in both speed and accuracy. For the looseness fault dataset, all networks met the speed requirements, with LightGBM providing superior accuracy.

Table 7. Fusion results of longitudinal available overload variation prediction models for different fault types.

Rudder	Damage	Stuck	Looseness
1st rudder	LightGBM	MLP	LightGBM
2nd rudder	LightGBM	MLP	LightGBM
3rd rudder	CatBoost	MLP	LightGBM
4th rudder	CatBoost	MLP	LightGBM

4.3. Prediction Model for $n_y^{\xi}(k)$ Results and Analysis

We combined the longitudinal available overload variation prediction models derived from the MLP, LightGBM, and CatBoost networks, and the fusion model with the analytical model to develop various multi-models for predicting the longitudinal available overload of a commercial subsonic aircraft with actuator faults. The box plot of the relative error distribution for different multi-models is shown in Figure 7. The wider the box corresponding to the relative error on the vertical axis, the more the test results were distributed within that error range. The red line represents a 5% relative error, the tolerance threshold in the aerospace industry [38]. As seen in Figure 7, the relative errors of the hybrid models based on the fusion model and LightGBM network were all within 5%, with most points having errors below 3%, meeting the aerospace industry's 5% tolerance requirement. However, some test points in the hybrid models based on MLP and CatBoost networks exceeded the 5% tolerance. Statistical analysis showed that test points with prediction errors greater than 3% were concentrated in the dataset with 60% defective actuators. This is because, under severe fault conditions, the aerodynamic configuration of the commercial subsonic aircraft changed more drastically, leading to significant variations in longitudinal available overload. Extracting these drastic changes from flight state data became more challenging, resulting in relatively larger errors.

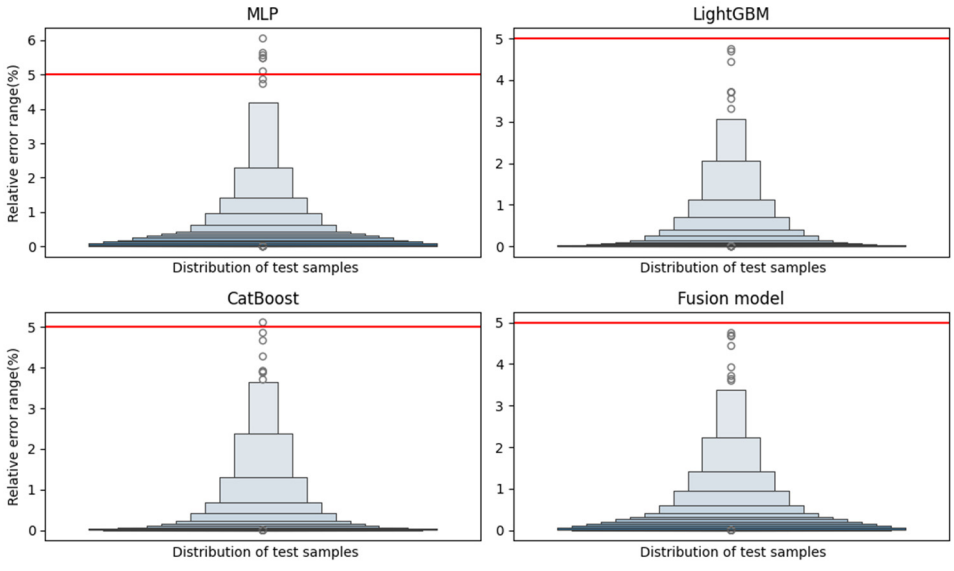

Figure 7. Relative error distribution of different multi-models for predicting $n_y^{\xi}(k)$.

The MAPE, MAE, and average prediction time per data point for the aforementioned hybrid models on the test set were statistically analyzed, as shown in Table 8. From Table 8, the following observations can be made:

1. There was a significant reduction in average relative error compared to the LightGBM network, with the smallest maximum relative error among the four models.

2. There was an enhanced prediction speed compared to MLP and LightGBM, with single dataset prediction times under 500 ms, meeting real-time requirements.

Table 8. Comparison of longitudinal available overload prediction models.

Metric	MLP	LightGBM	CatBoost	Fusion Model
Mean relative error	0.023%	0.067%	0.025%	0.046%
Maximum relative error	6.05%	4.75%	5.11%	4.75%
Mean prediction time (ms)	566.81	467.58	279.58	431.71

4.4. Comparison of Different Methods

The comparison of the accuracy, speed, and memory requirements for onboard applications, and the applicability of the different methods are presented in Table 9, where the speed results were influenced by computer performance, and the results for traditional analytical methods were based on all datasets tested in Table 2. From Table 9, we can draw the following conclusions:

1. Our method exhibited a significant improvement in accuracy compared to traditional methods. The traditional analytical method displayed substantial errors in the tests with the datasets from Table 2, primarily due to its reliance on aerodynamic models that are inaccurate under fault conditions, leading to larger discrepancies as the severity of the fault increases.
2. Although the prediction speed of our method was somewhat lower than that of traditional methods, the average time remained below 500 ms, thereby meeting the requirements for rapid predictions.
3. Our method demanded more memory on the onboard system compared to traditional analytical methods, but it required less memory than using a single MLP network.
4. The predictable range of our method was constrained by the datasets used, which included limitations in fault types, severity levels, and variations in flight parameters. Traditional overload analytical methods are restricted by the range of aerodynamic models; once this range is exceeded, the errors increase rapidly.

Table 9. Comparison of different methods.

		Maximum Relative Error	Mean Relative Error	Mean Prediction Time (ms)	Memory Requirement	Predictable Range
Multi-model		4.75%	0.046%	431.71	493 Mb	Constrained by the scope of the dataset
Traditional analytical method		49.50%	13.16%	2.18	23.7 kb	Constrained by the applicability of aerodynamic model
Single machine learning network	MLP	6.05%	0.023%	566.81	510 Mb	Constrained by the scope of the dataset
	LightGBM	4.75%	0.067%	467.58	358 Mb	Constrained by the scope of the dataset
	CatBoost	5.11%	0.025%	279.58	254 Mb	Constrained by the scope of the dataset

5. Conclusions

This paper proposes a multi-model that utilizes measurable flight parameters and fault information to forecast the longitudinal available overload of a commercial subsonic aircraft

under actuator faults overload. This multi-model comprises two components: one based on the analytical model of the commercial subsonic aircraft in a non-fault state for calculating the longitudinal available overload, and the other based on deep learning networks for predicting the longitudinal available overload variation with actuator faults. Simulation results demonstrate that the proposed multi-model achieves a relative error within 5% and delivers prediction results within 500 ms, validating the method's effectiveness and feasibility. Based on the analysis and experiments, the following conclusions can be drawn:

(1) By integrating the longitudinal available overload prediction models from the MLP deep learning network, CatBoost network, and LightGBM network under various actuator faults using specific rules, we significantly reduced the prediction error compared to traditional analytical methods, achieving a maximum relative error of less than 5%.
(2) Compared to individual machine learning network methods, our approach shows a significant decrease in the maximum relative error for longitudinal available overload predictions under actuator faults. The maximum relative error decreased by 1.3% compared to the single MLP network and by 0.36% compared to the single CatBoost network. Additionally, the prediction speed improved markedly, with an average prediction time reduction of 99.23 ms compared to the single MLP network.

The proposed method effectively addresses the challenge of quickly and accurately predicting longitudinal available overload in the presence of actuator faults under interference and uncertainty. This approach facilitates the rapid evaluation and precise prediction of an aircraft's longitudinal maneuvering capability, providing essential information support for trajectory planning and fault-tolerant control.

This study has several limitations. Firstly, our method requires substantial memory for onboard applications, which could exceed the maximum memory allocated to the algorithm during actual operation. In future research, we will optimize and streamline the network architecture of our method, using techniques such as knowledge distillation to develop a more lightweight network model. Furthermore, this study focuses on a specific type of commercial subsonic aircraft; future considerations include validating the proposed method on other variants of commercial subsonic aircraft.

Author Contributions: Conceptualization, S.S., Y.C. and B.J.; methodology, S.S.; validation, S.S., Y.C. and K.G.; formal analysis, S.S.; investigation, S.S. and Y.C.; data curation, S.S. and C.X.; writing—original draft preparation, S.S. and X.L.; writing—review and editing, S.S. and Y.C. All authors have read and agreed to the published version of the manuscript.

Funding: This research was funded by National Key Research and Development Program of China (No. 2023YFB3307102).

Institutional Review Board Statement: This study focuses on the development of techniques for commercial subsonic aircraft systems. The intention of this research is to enhance the performance and reliability of commercial subsonic aircraft systems, with the ultimate goal of contributing to peace, security, and defense. The authors consider the ethical implications of this research and ensure responsible use of the proposed technologies.

Informed Consent Statement: Not applicable.

Data Availability Statement: Data are available on request due to restrictions.

Conflicts of Interest: The authors declare no conflicts of interest.

References

1. Wu, J.; Yang, T.; Cao, X. A Typical Failure Mode and Effects Analysis for EMA Used for UAV and Guided Missile. *J. Phys. Conf. Ser.* **2021**, *1815*, 012043. [CrossRef]
2. Gao, Z.; Song, Y.; Wen, C.; Lewis, F.L. Asymptotic Output Tracking with Malfunctioning Actuators and Twisted/Biased Feedback. *IEEE Trans. Syst. Man Cybern. Syst.* **2023**, *54*, 1719–1729. [CrossRef]
3. Dong, H.; Chen, F.; Wang, Z.; Jia, L.; Qin, Y.; Man, J. An adaptive multisensor fault diagnosis method for high-speed train traction converters. *IEEE Trans. Power Electron.* **2020**, *36*, 6288–6302. [CrossRef]

4. Jlassi, I.; Cardoso, A.J.M. A single method for multiple IGBT, current, and speed sensor faults diagnosis in regenerative PMSM drives. *IEEE J. Emerg. Sel. Top. Power Electron.* **2019**, *8*, 2583–2599. [CrossRef]
5. Xie, D.; Lin, C.; Deng, Q.; Lin, H.; Cai, C.; Basler, T.; Ge, X. Simple Vector Calculation and Constraint-Based Fault-Tolerant Control for a Single-Phase CHBMC. *IEEE Trans. Power Electron.* **2024**. [CrossRef]
6. Xu, D.; Jiang, B.; Shi, P. Robust NSV fault-tolerant control system design against actuator faults and control surface damage under actuator dynamics. *IEEE Trans. Ind. Electron.* **2015**, *62*, 5919–5928. [CrossRef]
7. Gao, Z.; Song, Y.; Wen, C. Asymptotic Tracking Control with Bounded Performance Index for MIMO Systems: A Neuroadaptive Fault-Tolerant Proportional-Integral Solution. *IEEE Trans. Cybern.* **2023**, *54*, 4255–4266. [CrossRef]
8. Beck, J.; Cord, T. A framework for analysis of aircraft maneuverability. In Proceedings of the 20th Atmospheric Flight Mechanics Conference, Baltimore, MD, USA, 7–10 August 1995.
9. Goman, M.G.; Khramtsovsky, A.V.; Kolesnikov, E.N. Evaluation of aircraft performance and maneuverability by computation of attainable equilibrium sets. *J. Guid. Control Dyn.* **2008**, *31*, 329–339. [CrossRef]
10. Li, J.H.; Liu, X.S.; Feng, Y.H. Research on Performance Evaluation Methods of Vehicle Flight Control. *Ship Electron. Eng.* **2017**, *37*, 38–42.
11. Ma, W.H. Research on Evaluation Method of Guidance and Control Performance for Hypersonic Vehicle. *Aerosp. Control* **2012**, *30*, 7–12.
12. Liu, Y.W.; Wang, Y.J.; Liu, L.; Dong, S. Performance Evaluation of Control System Based on the Analytic Hierarchy Process. *Comput. Technol. Autom.* **2014**, *33*, 6–10.
13. Sang, B.; Guo, Y.; Shi, D.; Xu, W. Decision-theoretic roughset model of multi-source decision systems. *Int. J. Mach. Learn. Cybern.* **2018**, *9*, 1941–1954. [CrossRef]
14. Ma, K.; Zhang, H.; Wang, R.; Zhang, Z. Target tracking system for multi-sensor data fusion. In Proceedings of the 2017 IEEE 2nd Information Technology, Networking, Electronic and Automation Control Conference, Chengdu, China, 15–17 December 2017.
15. Stufflebeam, D. Evaluation models. *New Dir. Eval.* **2001**, *89*, 7–98. [CrossRef]
16. Yang, H.D.; Tuo, H.P. Calculation method of range for trajectory programmable aircraft. *Mod. Def. Technol.* **2018**, *46*, 35–40.
17. Traub, L.W. Range and endurance estimates for battery-powered aircraft. *J. Aircr.* **2011**, *48*, 703–707. [CrossRef]
18. Liu, W.J.; Wei, Z.X.; Zhang, Y.H.; Wu, Y.R. *Missile Flight Mechanics*, 1st ed.; Xidian University Press: Xi'an, China, 2014; pp. 65–99.
19. Qian, X.F.; Lin, R.X.; Zhao, Y.N. *Missile Flight Mechanics*, 1st ed.; Beijing Institute of Technology Press: Beijing, China, 2006; pp. 36–61.
20. Zhang, J.L.; Liu, K.; Fan, Y.Z.; She, Z.Y. Prediction and correction switching reentry guidance method based on neural network range estimation model. *Tactical Missile Technol.* **2020**, *5*, 93–100.
21. Wu, Z.X.; Zhang, N.; Gao, K.Y.; Peng, K. Flight trip fuel volume prediction based on random forest with adjustment to risk preference. *Acta Aeronaut. ET. Astronaut. Sin.* **2022**, *43*, 224–933.
22. Lei, X.B.; Wen, M.; Lei, D.Y.; Zhang, X. Prediction of Aircraft Normal Overload Extreme Value Based on Pearson-III Distribution. *J. Mech. Strength* **2018**, *40*, 106–110.
23. Zhang, W.Q.; Cheng, Y.H.; Yu, Z.Q.; Cao, R. Research of aircraft longitudinal available overload prediction method based on LSTM. *Flight Dyn.* **2023**, *41*, 23–29.
24. Al-Jarrah, O.Y.; Yoo, P.D.; Muhaidat, S.; Karagiannidis, G.K.; Taha, K. Efficient machine learning for big data: A review. *Big Data Res.* **2015**, *2*, 87–93. [CrossRef]
25. Zhang, P.T.; Han, Y.X.; Zhang, Z. *Theory and Practice of Aircraft System Identification*, 1st ed.; Aviation Industry Press: Beijing, China, 2019; pp. 60–89.
26. Spearman, C. The proof and measurement of association between two things. *Int. J. Epidemiol.* **2010**, *39*, 1137–1150. [CrossRef] [PubMed]
27. Prabhu, S.; Anitha, G. An innovative analytic redundancy approach to air data sensor fault detection. *Aeronaut. J.* **2020**, *124*, 346–367. [CrossRef]
28. Cao, P.P.; Ma, J.Q.; Yang, G.Z.; Feng, T.N.; Wang, X. Typical electrode discharge acoustic signal denoising in oil based on improved VMD. *J. Meas. Sci. Instrum.* **2024**, *15*, 1–12.
29. Rtayli, N.; Enneya, N. Selection features and support vector machine for credit card risk identification. *Procedia Manuf.* **2020**, *46*, 941–948. [CrossRef]
30. Shah, F.P.; Patel, V. A review on feature selection and feature extraction for text classification. In Proceedings of the 2016 International Conference on Wireless Communications, Signal Processing and Networking (WiSPNET), Chennai, India, 23–25 March 2016; IEEE: Piscataway, NJ, USA, 2016; pp. 2264–2268.
31. Zhang, J.; Guo, Y.F.; Pan, D.Z.; Yang, K.M.; Lian, X.J.; Yao, J.F. Effective doping concentration theory: A new physical insight for the double-RESURF lateral power devices on SOI substrate. *IEEE Trans. Electron Devices* **2018**, *65*, 648–654. [CrossRef]
32. Sharma, A.; Singh, B. AE-LGBM: Sequence-based novel approach to detect interacting protein pairs via ensemble of autoencoder and LightGBM. *Comput. Biol. Med.* **2020**, *125*, 103964. [CrossRef]
33. Dorogush, A.V.; Ershov, V.; Gulin, A. CatBoost: Gradient boosting with categorical features support. *arXiv* **2018**, arXiv:1810.11363.
34. Huang, H.; Zhao, X.; Zhang, X. Intelligent guidance and control methods for missile swarm. *Comput. Intell. Neurosci.* **2022**, *2022*, 8235148. [CrossRef]

35. Anyanwu, G.O.; Nwakanma, C.I.; Lee, J.M.; Kim, D.S. Optimization of RBF-SVM kernel using grid search algorithm for DDoS attack detection in SDN-based VANET. *IEEE Internet Things J.* **2022**, *10*, 8477–8490. [CrossRef]
36. Taheri, S.; Razban, A. Learning-based CO_2 concentration prediction: Application to indoor air quality control using demand-controlled ventilation. *Build. Environ.* **2021**, *205*, 108164. [CrossRef]
37. Plevris, V.; Solorzano, G.; Bakas, N.P.; Ben Seghier, M.E. Investigation of Performance Metrics in Regression Analysis and Machine Learning-Based Prediction Models. In Proceedings of the 8th European Congress on Computational Methods in Applied Sciences and Engineering (ECCOMAS Congress 2022), Oslo, Norway, 5–9 June 2022.
38. Sun, C.; Li, H.; Dui, H.; Hong, S.; Sun, Y.; Song, M.; Cai, D.; Zhang, B.; Wang, Q.; Wang, Y.; et al. A multi-model architecture based on deep learning for aircraft load prediction. *Commun. Eng.* **2023**, *2*, 47. [CrossRef]